HYDROGEN-INDUCED FRACTURE PHENOMENA IN A BCC TITANIUM ALLOY

W. W. Gerberich, K. Jatavallabhula, K. A. Peterson, and C. L. Jensen

Department of Chemical Engineering and Materials Science
University of Minnesota, Minneapolis 55455

ABSTRACT

In Ti-30 Mo, effects of hydrogen on internal stress, fracture stress and fracture surface morphology suggest a stress-induced embrittling phase such as ω phase. The ductile-brittle transition increases and fracture stress decreases almost linearly with hydrogen additions. Such results may be used in a fracture mechanics analysis to predict threshold stress intensities with no adjustable parameters.

KEYWORDS

Titanium; all-beta alloy; internal stress; fracture stress; ductile-brittle transition; stress-intensity thresholds, hydrogen embrittlement.

INTRODUCTION

The desire to understand the stress-corrosion-cracking and hydrogen embrittlement resistance of titanium alloys has prompted scores of investigations into all-alpha and α/β titanium alloys over the last three decades. Significantly, there have been far fewer investigations on all-beta alloys and almost no fracture mechanics investigations of stable β alloys. The importance of understanding the effect of hydrogen on the resistance of the β phase to fracture is two-fold:

(i) to further development of metastable and stable β alloys;
(ii) to incorporation of any β phase embrittlement into how hydrogen and hydrogen-producing environments affect α/β alloys.

Although there have been a large number of studies on phase transformations and morphology (Williams, 1973) and the effects of these on the mechanical properties of metastable β alloys (Jaffee, 1973), one of the few studies to evaluate a stable β alloy was that of Paton and Williams (1974). They reported that the β phase can absorb hydrogen up to 4000 ppm (wt) with no evidence of hydride formation but that considerably larger concentrations can cause it to crumble. It is important to know if the β phase is susceptible to relatively small concentrations of hydrogen (e.g. < 1000 ppm) and, if so, what the mechanism of embrittlement is. For that reason, we selected a Ti-30 Mo (wt %) alloy in thick plate form so that a series of mechanical tests, including tension, compression, impact, slow-notch bend and fracture toughness, could be conducted.

EXPERIMENTAL PROCEDURES

The Ti-30 Mo was received in the beta-worked condition. Subsequent annealing for four hours at 1000°C and cooling at 10°C/min produced a coarse structure with a grain size ranging from 85-100μm. Vacuum annealing at 10^{-5} torr produced a hydrogen concentration of 102 ppm (wt). Higher hydrogen concentrations for smaller compression cylinders or Charpy V-notch specimens were achieved by cathodically charging vacuum annealed samples. Homogenization of the hydrogen in compression and V-notch samples was accomplished by baking at 200°C for six hours and 12 hours, respectively. For higher hydrogen concentrations in the larger compact tension specimens, gas-phase charging was formed by first holding for one hour at 870°C in an argon-hydrogen atmosphere at 152 mm partial pressure of hydrogen. This was then reduced to either 4.2 mm or 1.3 mm of hydrogen for an additional six hours. Compression cylinders with a height to diameter ratio of 2.5 were machined in the longitudinal orientation and tested uniaxially under a strain rate of 3.32×10^{-4} sec^{-1}. For internal stress measurements, the crosshead of the test machine was stopped and a decremental unloading technique was employed. Charpy V-notch specimens were taken in the L-T orientation and tested in slow bending. A crosshead rate of 4.2×10^{-4} cm. sec^{-1} was used in a four point bend jig with a 1.27 cm bending arm. Compact tension specimens were machined and fatigue precracked according to ASTM 399 procedures. For sustained load-cracking, monitoring was accomplished with a calibrated crack-opening displacement gage. Threshold stress intensities were achieved by stepping up the stress intensity in 2MPa-$m^{\frac{1}{2}}$ units with hold times of six to eleven hours.

RESULTS

For hydrogen concentrations from 22 up to 1400 ppm (wt), yield strengths were measured in compression at seven different test temperatures. As seen in Fig. 1, there is a rapid increase in yield strength with decreasing temperature. The effect of increasing hydrogen concentration on yield strength is small at temperatures near 300 K but increases at lower temperatures where a 300 ppm hydrogen addition increased the strength by 250 MPa. It is also seen that this effect of larger hydrogen concentrations increasing strength plateaus out and perhaps even decreases at higher concentrations.

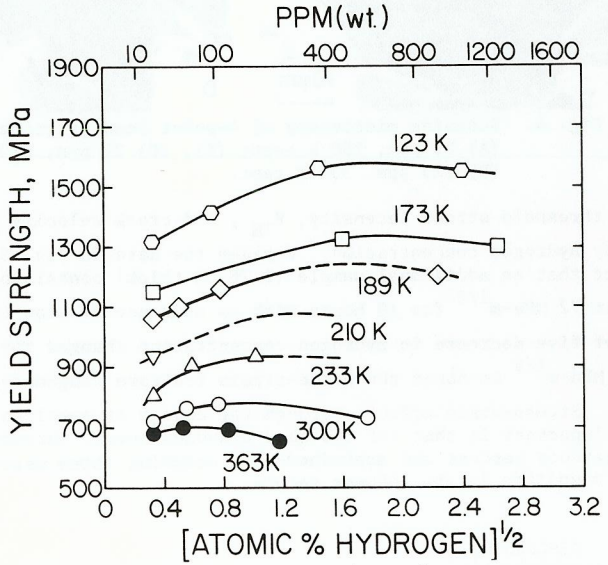

Fig. 1. Hydrogen concentration and test temperature effects on compressive yield strength.

From the positive and negative stress relaxation testing, the internal stresses were measured for two hydrogen levels, 22 and 102 ppm. Surprisingly, there was a very large dependence of internal stress, σ_i, on test temperature. This is shown in Fig. 2 where σ_i increased by nearly a factor of three as test temperature decreased from 350 to 100 K. For the two hydrogen levels examined, those with the higher concentration had internal stresses from about 75 to 100 MPa greater; this roughly corresponds to the yield strength increment in Fig. 1. The yield stress is normally thought to be made up of internal stress, σ_i, and thermally-activated flow stress, σ^*, terms given by

$$\sigma_{ys} = \sigma_i + \sigma^*_{(T,\dot{\varepsilon})} \quad (1)$$

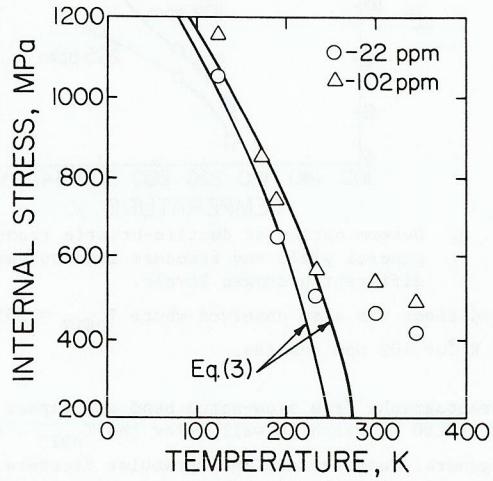

Fig. 2. Effect of test temperature on internal stress, σ_i, for two internal hydrogen levels.

According to the observed yield and internal stresses in Figs. 1 and 2, Eq. (1) would indicate that $\sigma^*_{(T,\dot{\varepsilon})}$ was nearly constant on the order of 260 MPa. Since the yield and internal stress were affected by about the same amount, the hydrogen effect appears to be in the internal stress component and not in the thermal stress component, at least for small hydrogen additions.

Fracture loads from notch bend samples with three hydrogen levels are shown in Fig. 3. Superimposed upon these curves are two general yield curves calculated from the von Mises yield criterion for 22 and 102 ppm hydrogen. The curve for 225 ppm falls in between these two for temperatures in the range of 240 to 360 K. It is seen that the ductile brittle transition temperature, T_{DBTT}, increases by about 100 K with only 200 ppm addition. Correspondingly, the fracture load and hence the fracture stress decreases with increasing hydrogen. A similar shift in T_{DBTT}

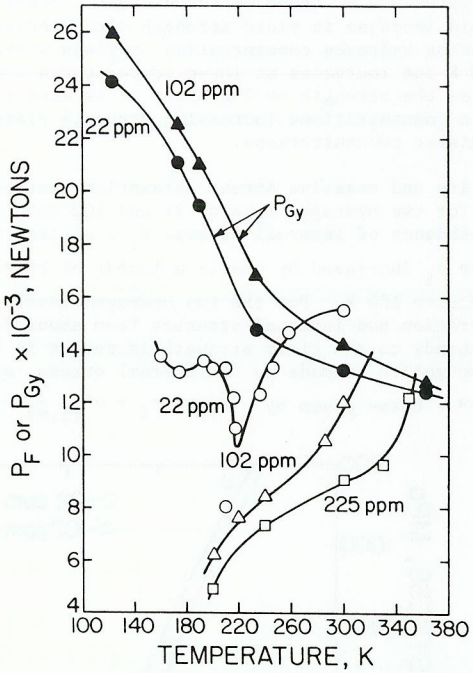

Fig. 3. Determination of ductile-brittle transitions from general yield and fracture load curves for three different hydrogen levels.

under impact conditions was also observed where $T_{DBTT} \simeq 355K$ for 22 ppm samples and $T_{DBTT} \simeq 449$ K for 102 ppm samples.

The resulting fractography from slow-notch bend and impact testing was the same. Typical results at 160 K, which is well below the T_{DBTT}, are shown in Figs. 4(a) and 4(b). The general features are intergranular fracture, microvoid coalescence and transgranular cleavage. In many instances there appeared to be a grain boundary phase, for example between the cleavage and microvoid coalescence at the right of Fig. 4(a). In addition, there was a fine structure mixed with the cleavage that suggested very shallow dimples on the order of 5000 Å in dimension. This was particulary evident at the bottom left of Fig. 4(a). For comparison, Figs. 4(b) through 4(d) show fractography from samples fractured at about 30 K below the T_{DBTT} for samples containing 22 and 225 ppm hydrogen. There were no particular differences noted and the same grain boundary phase (4b), cleavage appearance (4c,d) and mottled structure mixed in with cleavage rivers (4b, top) were noted. The "cleavage rivers" in Fig. 4(c) could be mistaken for intersecting sets of planar slip lines or twins except that close examination reveals a "scalloped appearance". Although the micrographs shown here emphasize the cleavage aspects, it was estimated that there was about 20 percent cleavage, 30 percent microvoid coalescence and 50 percent intergranular fracture at temperatures below and near T_{DBTT}.

Threshold stress intensity and crack growth rate data were evaluated on compact tension samples at two hydrogen levels and two thicknesses. Results in Fig. 5

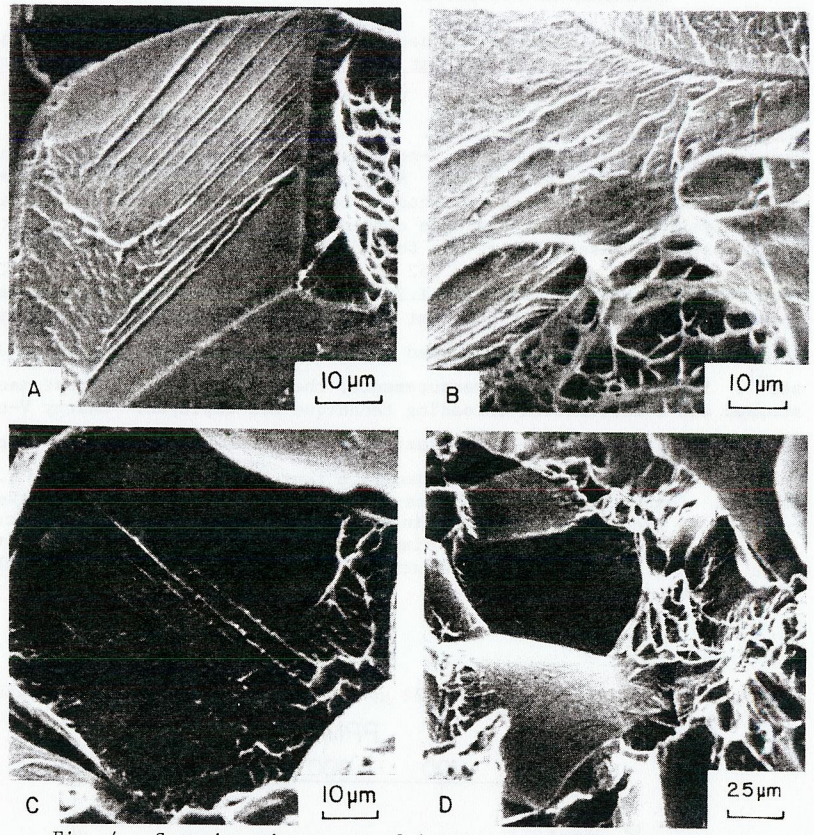

Fig. 4. Scanning microscopy of 4-point bend fracture surfaces: (A) 22 ppm, 160 K test; (B), (C) 22 ppm, 210 K test; (D) 225 ppm, 330 K test.

show that threshold stress intensity, K_{TH}, and crack velocity da/dt, are strongly affected by hydrogen concentration. Besides the data in Fig. 5, it should be pointed out that an additional sample (1.78 cm thick) containing 110 ppm hydrogen was held at 72 MPa-$m^{1/2}$ for 18 hours with no evidence of slow crack growth. Thus, a factor of five decrease in hydrogen concentration changed the threshold level from 31.2 MPa-$m^{1/2}$ to about the plane-strain fracture toughness level, $K_{IC} \simeq 76$ MPa-$m^{1/2}$. Stress-state effects through the change in specimen thickness were nearly as important in that for the same hydrogen level, thresholds were increased by about seventy percent and sustained-load cracking rates were decreased by orders of magnitude in the thinner sample.

DISCUSSION

From the measurements made, one can reach some very concrete conclusions about hydrogen effects on yield strength, fracture and slow crack growth but only limited

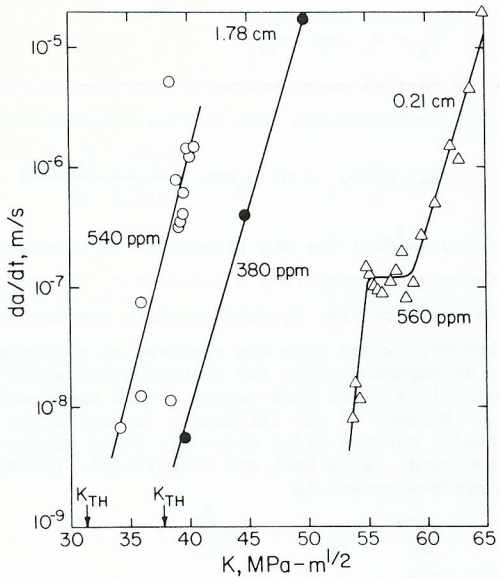

Fig. 5. Crack growth rate vs. stress intensity for thick and thin compact tension specimens containing various hydrogen levels.

hypotheses on either internal stress or fracture mechanisms.

Internal Stress Hypothesis

The one interesting feature of compression and tensile testing was that the internal stress was so greatly dependent upon test temperature. This was somewhat unexpected in this BCC alloy which was thought to be completely stable. There was little previous evidence that σ_i would behave this way for this BBC alloy and the question as to why the long-range internal stress should depend so strongly on test temperature was puzzling. The most likely possibility is the ω-phase transformation. Cold stage electron microscopy observations of the athermal $\beta \rightarrow \omega$ transformation have been made by DeFontaine, Paton and Williams (1971) and strain-induced ω transformation in a Ti-15 Mo alloy has been observed by Wood (1963). We will term the respective transformation temperatures as T_{ω_A} and T_{ω_ε}. With regards to the results of Ono, and colleagues (1972), they concluded that the most probable explanation of internal friction peaks was massive formation of ω phase resulting with the aid of applied stress. This is very plausible since the lattice shuffles involved are small, the reaction is highly reversible (Cook, 1974) and the misfits are relatively small (Williams, 1973). Since the temperature regime for the internal friction peak was very broad, we will denote two temperatures, the start of the peak, $T_{\omega_{\sigma_s}}$, and the peak itself, $T_{\omega_{\sigma_p}}$. All of the data associated with the $\beta \rightarrow \omega$ transformation are shown in Fig. 6. The assumption we will make here is that the long range internal stress is largely due to a stress-induced ω phase which is hard compared to the β phase. To get a first order estimate of the effect on internal stress, Cook's (1974) theory of the omega transformation is used from which the volume fraction would be

$$f_\omega = \frac{2x_i^*}{d_\omega} \simeq \frac{2\cos^{-1}(\hat{A}^*/\hat{A}_\omega)}{\pi} \tag{2}$$

where $2x_i^*$ is the particle size, d_ω the periodicity, $\hat{A}^*$ the potential barrier and $\hat{A}_\omega$ the amplitude of the metastable state minima. Taking the simplest possible form for the temperature dependence to be $\hat{A}^*/\hat{A}_\omega \approx T/T_{\omega_{\sigma_s}}$ and that σ_i is proportional to the volume fraction of ω phase, one obtains

$$\sigma_i \simeq f_\omega \sigma_\omega \simeq \frac{2}{\pi}\sigma_\omega \cos^{-1}\{T/T_{\omega_{\sigma_s}}\} \tag{3}$$

From aging characteristics of unstable β alloys, (Ohtani, and colleagues, 1973), it was estimated that the yield strength of the ω phase was about 1500 MPa. This in conjunction with $T_{\omega_{\sigma_s}} \simeq 250$ K, as estimated from Fig. 6, gave the bottom solid curve in Fig. 2. The agreement is good considering the approximations. If one now argues that the effect of hydrogen additions is to induce the ω phase transformation, then a shift in $T_{\omega_{\sigma_s}}$ to 280 K allows the upper curve in Fig. 2 to approximate the internal stress. If this is correct, then it would appear that 80 ppm hydrogen raised the transformation temperature by about 30 K.

Fracture Phenomena

From the general yield and fracture loads in Fig. 3, the fracture stresses were determined from the Orowan criterion, which is

$$\text{pcf} \cdot \sigma_{ys}\Big|_{T,\dot{\varepsilon}_p} = \sigma_{11}^{max} \geq \sigma_f^* \tag{4}$$

Here, pcf is the plastic constraint factor, $\sigma_{ys}\Big|_{T,\dot{\varepsilon}_p}$ is the uniaxial yield stress at the temperature and strain rate of interest, σ_{ii}^{max} is the maximum stress at the discontinuity and σ_f^* is the fracture stress. The plastic constraint of 2.44

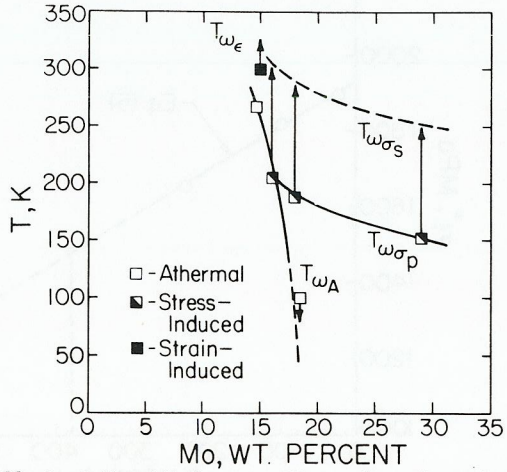

Fig. 6. Effect of Mo additions to Ti on the athermal, stress-induced and strain-induced $\beta \rightarrow \omega$ transformation temperatures.

for this elastic-plastic material was determined for four point bend testing using Knott's (1973) results. The resulting fracture stresses are seen in Fig. 7 to decrease linearly with increasing hydrogen concentration levels. From a least squares fit, one obtains

$$\sigma_f^* = \sigma_{f_o}^* - \alpha' C_H \tag{5}$$

where $\sigma_{f_o}^*$ is 1926 MPa and α' is 1.18 MPa/ppm (wt). In the time frame of these slow-notch bend tests, it is assumed that $C_H \approx C_o$. This was verified in that the T_{DBTT} shift was nearly identical under impact conditions. At some hydrogen concentration one would expect that the curve would tend towards a horizontal plateau since Eq. (5) indicates that 1650 ppm is sufficient to reduce the fracture stress to zero.

What is the role of hydrogen in reducing σ_f^* ? Partially because of the metallographic and fractographic observations and partially because of the internal stress results, the most promising candidate is stress-induced ω. The hydrogen could simply aid in promoting the ω transformation and thus decrease σ_f^*. Given that hydrogen reduces σ_f^* by this or another mechanism, it was of interest to apply the results to the fracture mechanics observations.

Threshold Modelling

Two approaches will be used, elastic stress field and plastic constraint models (Gerberich and Chen, 1975). In a coarse grained material, the hypothesis is that σ_f^* is achieved over two grain diameters (Ritchie and colleagues, 1973). For an elastic criteria, this gives

$$K_{TH} \approx \sigma_f^* \sqrt{2\pi r} \tag{6}$$

with σ_f^* given by Eq. (5) and $r \approx 2d$, where d is the grain size of 92μm. Since C_H would be dependent on the concentrating effect of the stress tensor, σ_{ii}, this gives

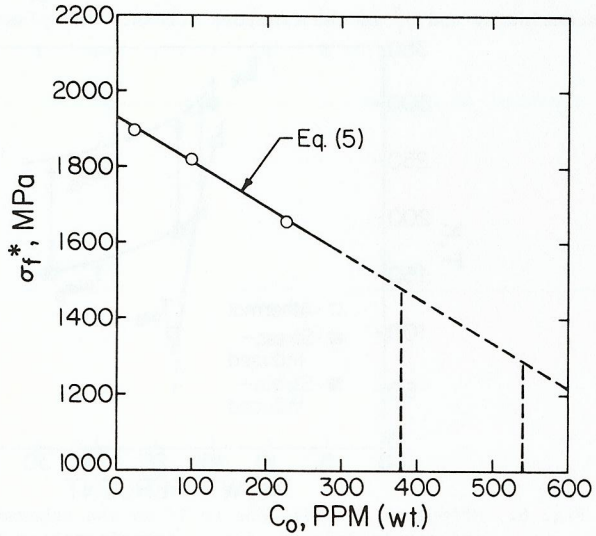

Fig. 7. Effect of hydrogen concentration on the fracture stress of Ti-30 Mo.

$$C_H = C_o \exp\left\{\frac{\sigma_{ii} \bar{V}_H}{3RT}\right\} \tag{7}$$

where $\bar{V}_H$ is the partial molar volume of hydrogen in the alloy. With the value given for σ_{ii} by Gerberich and Chen (1975), and Eqs. (5-7), one obtains

$$K_{TH} \approx \left[\sigma_{f_o} - \alpha' C_o \exp\left\{\frac{2(1+\nu)\, K_{TH}\, \bar{V}_H}{3\sqrt{4\pi d}\; RT}\right\}\right]\sqrt{4\pi d} \tag{8}$$

with $\bar{V}_H$ near 1.5 cm^3/mol for BCC titanium. In conjunction with all other parameters which are independently measured, a value of C_o may be simply calculated for a given K_{TH}. As shown in Fig. 8, this predicts the data very well except that it predicts a threshold where none was observed at a hydrogen concentration of 100 ppm. This is as expected since the elastic model would break down well before this stress intensity level. For this reason it was necessary to invoke an elastic-plastic criterion. Because of the difficulty in specifying crack-tip radii and hence plastic constraint factors using slip-line field analyses, a more experimental approach was developed. With Hahn and Rosenfield's (1966) experimental relationship for pcf, the maximum stress is

$$\sigma_{yy}^{max} \approx \sigma_{ys}\left[1 + \alpha\left(\frac{K_I}{\sigma_{ys}}\right)\right] \tag{9}$$

where $\alpha \approx 12.55 m^{-1/2}$. For a fracture criterion, this becomes

$$K_I \approx [\sigma_f^* - \sigma_{ys}]\alpha^{-1} \tag{10}$$

If there were no hydrogen concentration effects, Eq. (10) gives the plane strain fracture toughness, K_{IC}. With time, however, σ_f^* is modified by hydrogen concentrating at the crack tip via the hydrostatic tensile stress,

$$\frac{\sigma_{ii}}{3} = \sigma_{ys}\left[\frac{\sigma_{yy}^{max}}{\sigma_{ys}} - \frac{1}{2}\right] \approx \frac{\sigma_{ys}}{2} + \alpha K_I \tag{11}$$

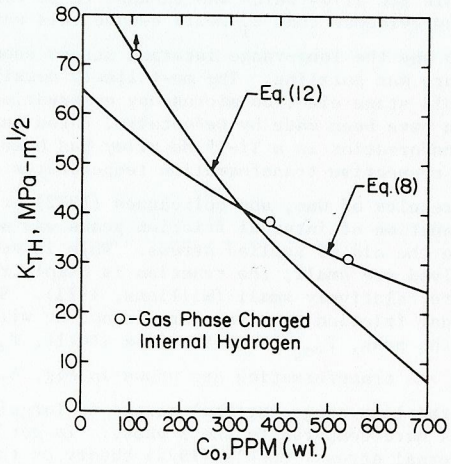

Fig. 8. Prediction of hydrogen concentration on threshold stress intensities by elastic and elastic-plastic models.

Combining Eqs. (5), (7), (10) and (11) leads to

$$K_{TH} \simeq \frac{1}{\alpha} \left[\sigma_{f_o}^{*} - \sigma_{ys} - \alpha' C_o \exp\left\{\frac{\left(\frac{\sigma_{ys}}{2} + \alpha K_{TH}\right)\bar{V}_H}{RT}\right\}\right] \quad (12)$$

With the same value of 1.5 cm^3/mol for $\bar{V}_H$ and no adjustable parameters, the curve in Fig. 8 predicts the K_{TH} value reasonably well and the observed fracture toughness of 76 MPa-$m^{1/2}$.

CONCLUSIONS

1. The yield strength of a BCC Ti-30 Mo alloy first increases and then decreases with increasing hydrogen additions.
2. For every ppm (wt) internal hydrogen addition, the ductile-brittle transition temperatures increased about 0.48°, and fracture stress decreased about 1.18 MPa.
3. The internal stress, as measured by the decremental unloading technique, increased rapidly from about 400 MPa to 1000 MPa as temperature decreased.
4. Hydrogen induced sustained-load cracking and thresholds near 30 MPa-$m^{\frac{1}{2}}$ are observed for hydrogen concentrations on the order of 440 ppm (wt).
5. Fracture mechanics analyses can predict plane strain thresholds from the effect of hydrogen on the fracture stress.

ACKNOWLEDGEMENT

The authors would like to express their thanks to W. Kerr of the Air Force Materials Laboratory for providing gas-phase charging and to the support of the Air Force Office of Scientific Research through contract AFOSR 78-3133.

REFERENCES

Cook, H. E. (1974). Acta Metallurgica, 22, 239-247.
DeFontaine, D., N. E. Paton and J. C. Williams (1971). Acta Met., 19, 1153-1162.
Gerberich, W. W. and Y. T. Chen (1975). Met. Trans., 6A, 271-278.
Hahn, G. T. and A. R. Rosenfield (1966). Trans. ASM, 59, 909-919.
Jaffee, R. I. (1973). Titanium Science and Technology, 3, Plenum Press, New York. 1665-1693.
Knott, J. F. (1973). Fundamentals of Fracture Mechanics, John Wiley & Sons, New York.
Ohtani, S., M. Nishigaki and T. Nishimura (1973). Titanium Science and Technology, 3, Plenum Press, New York, 1945-1956.
Ono, K., L. A. Rosales, S. Motokura and A. W. Sommer (1972). Mechanical Behavior of Materials, I, Soc. of Materials Science, Japan, Kyoto, 66-77.
Paton, N. E. and J. C. Williams (1974). Hydrogen in Metals, ed. by Bernstein and Thompson, American Soc. for Metals, Metals Park, Ohio, 409-432.
Ritchie, R. O., J. F. Knott and J. R. Rice (1973). J. Mech. Phys. Solids, 21, 395-410.
Williams, J. C. (1973). Titanium Science and Technology, 3, Plenum Press, New York, 1433-1494.
Wood, R. M. (1963). Acta Metallurgica, 11, 907-914.